

RESEARCH ARTICLE

10.1002/2013JG002569

Key Points:

- Stepwise and gradual warming enhance ecosystem C sink at the tundra site
- Greater winter soil warming shifts ecosystem net C sink to net source
- Warming tundra can provide positive feedback to climate change

Supporting Information:

- Readme
- Figures S1 and S2
- Table S1

Correspondence to:

J. Li,
jianweili.2@gmail.com

Citation:

Li, J., Y. Luo, S. Natali, E. A. G. Schuur, J. Xia, E. Kowalczyk, and Y. Wang (2014), Modeling permafrost thaw and ecosystem carbon cycle under annual and seasonal warming at an Arctic tundra site in Alaska, *J. Geophys. Res. Biogeosci.*, 119, 1129–1146, doi:10.1002/2013JG002569.

Received 11 NOV 2013

Accepted 16 MAY 2014

Accepted article online 22 MAY 2014

Published online 13 JUN 2014

Modeling permafrost thaw and ecosystem carbon cycle under annual and seasonal warming at an Arctic tundra site in Alaska

Jianwei Li¹, Yiqi Luo¹, Susan Natali^{2,3}, Edward A. G. Schuur², Jianyang Xia¹, Eva Kowalczyk⁴, and Yingping Wang⁴

¹Department of Microbiology and Plant Biology, University of Oklahoma, Norman, Oklahoma, USA, ²Department of Biology, University of Florida, Gainesville, Florida, United States, ³Woods Hole Research Center, Falmouth, Massachusetts, United States, ⁴CSIRO Marine and Atmospheric Research, Centre for Australian Weather and Climate Research, Aspendale, Victoria, Australia

Abstract Permafrost thaw and its impacts on ecosystem carbon (C) dynamics are critical for predicting global climate change. It remains unclear whether annual and seasonal warming (winter or summer) affect permafrost thaw and ecosystem C balance differently. It is also required to compare the short-term stepwise warming and long-term gradual warming effects. This study validated a land surface model, the Community Atmosphere Biosphere Land Exchange model, at an Alaskan tundra site, and then used it to simulate permafrost thaw and ecosystem C flux under annual warming, winter warming, and summer warming. The simulations were conducted under stepwise air warming ($2^{\circ}\text{C yr}^{-1}$) during 2007–2011, and gradual air warming ($0.04^{\circ}\text{C yr}^{-1}$) during 2007–2056. We hypothesized that all warming treatments induced greater permafrost thaw, and larger ecosystem respiration than plant growth thus shifting the ecosystem C sink to C source. Results only partially supported our hypothesis. Climate warming further enhanced C sink under stepwise (6–15%) and gradual (1–8%) warming scenarios as followed by annual warming, winter warming, and summer warming. This is attributed to disproportionately low temperature increase in soil (0.1°C) in comparison to air warming (2°C). In a separate simulation, a greater soil warming (1.5°C under winter warming) led to a net ecosystem C source (i.e., $18\text{ g C m}^{-2}\text{ yr}^{-1}$). This suggests that warming tundra can potentially provide positive feedbacks to global climate change. As a key variable, soil temperature and its dynamics, especially during wintertime, need to be carefully studied under global warming using both modeling and experimental approaches.

1. Introduction

A large carbon (C) reservoir (1672 pg C) [Tarnocai et al., 2009] in the Arctic and boreal regions of the Northern Hemisphere will encounter the most pronounced climate warming ($7\text{--}8^{\circ}\text{C}$) this century [Arctic Climate Impact Assessment (ACIA), 2004]. Frozen C within permafrost zone can be stimulated by warming via microbial decomposition and released to the atmosphere in a large quantity and spatial extent [Schuur et al., 2008; Tarnocai et al., 2009; Harden et al., 2012]. Thawing permafrost therefore can increase the amplitude of the C cycle and exert an important influence on the future landscape level C balance [Zimov et al., 1996]. It was recently hypothesized that the permafrost thawed carbon can be up to 147–436 pg C from 2050 to 2100 [Harden et al., 2012; Schuur et al., 2013]. Other Earth System models simulated a 62 pg C loss as permafrost C feedback to climate warming [Koven et al., 2011]. The additional warming is about $0.04\text{--}0.23^{\circ}\text{C}$ at the end of this century [Schneider von Deimling et al., 2012] and $0.2\text{--}1.7^{\circ}\text{C}$ warming in two centuries [MacDougall et al., 2012]. At the ecosystem level, warming tundra may increase ecosystem C accumulation and act as a C sink, but these estimates still possess large uncertainty such that it can also be a large C source [Waelbroeck et al., 1997; Khvorostyanov et al., 2008b; Hayes et al., 2011; Schaefer et al., 2011; McGuire et al., 2012]. Understanding how permafrost thaw is affected under climate warming and how it can feedback to climate warming via ecosystem C exchange will essentially increase our capacity to predict global C cycling in a warmer world.

Permafrost thawing as a result of warming alters energy, water, and carbon fluxes at the surface layers [Osterkamp et al., 2009]. The active layer thickness (ALT), defined as the depth of maximum seasonal penetration of the 0°C isotherm [Hinkel et al., 1997; Nelson, 2003], is a seasonally thawed surface layer due to

annual thawing and freezing in areas underlain by permafrost. Climate warming has deepened the ALT by ~ 7.5 cm/yr in the Tibetan region [Wu and Zhang, 2010] and is projected to increase ALT more than 30% during this century across tundra area in the Northern Hemisphere [Anisimov *et al.*, 1997, 2002; Dankers *et al.*, 2011]. On the other hand, growing season gross primary productivity (GPP) and net ecosystem exchange (NEE, i.e., $GPP + R_{eco}$) may also increase as permafrost is degraded, in spite of less change in annual or growing season ecosystem respiration (R_{eco} , negative value) [Belshe *et al.*, 2012; Trucco *et al.*, 2012]. Warming can thus increase the plant C pool [Natali *et al.*, 2012] at a site level and, on the other hand, accelerate litter mass loss and soil respiration across multiple sites [Lu *et al.*, 2012]. Understanding the responses of both plant growth and respiration and their association with permafrost thaw under warming is necessary to reveal the underlying mechanisms that regulate ecosystem fluxes and C storage capacity of tundra ecosystems.

Future warming scenarios are not uniform across high-latitude regions and seasons. Site-specific differences such as climate and soil may result in varying responses to the same warming scenario, and sites may also experience temperature increase at different seasons such as winter warming or summer warming. Winter warming has been more pronounced in high-latitude regions during this century [Osterkamp, 2007; Xia *et al.*, 2014]. Several lines of evidence show great seasonal variations in temperature sensitivity of microbial enzyme activity [Brzostek and Finzi, 2012] and nitrogen cycling [Weedon *et al.*, 2012] in high-latitude soils, which will exert a strong control in regulating tundra ecosystem response to warming [Grogan and Chapin, 1999; Chapin *et al.*, 2000]. Climate had strong effects on belowground respiration in both winter and summer seasons, while vegetation type was the principal control of belowground respiration in summer, suggesting that seasonality is a critical factor in regulating climate and vegetation-type effects on ecosystem C efflux and net C balance in Arctic ecosystems [Grogan and Chapin, 1999]. Growing season length, spring warming, and earlier snowmelt can regulate land-atmosphere C exchange and ecosystem C sequestration in high-latitude tundra ecosystems [Humphreys and Lafleur, 2011; Parmentier *et al.*, 2011; Tang and Zhuang, 2011]. Summer warming and increased winter snow cover affected *Sphagnum fuscum* growth, structure, and production in a subarctic bog, which altered the C balance of northern peatlands [Dorrepaal *et al.*, 2004]. It is also estimated that wintertime respiration with warming may offset the growing season C gain and thus alter annual C balance [Natali *et al.*, 2011; Belshe *et al.*, 2012; Trucco *et al.*, 2012; Belshe *et al.*, 2013].

Permafrost ecosystem C balance depends on the sensitivity of biological processes (i.e., photosynthesis and respiration), which can be further regulated by physical changes (i.e., snow cover, ice, and water) as permafrost thaws. For example, the altered rate and timing of snow cover termination can regulate permafrost thaw depth [Frauenfeld *et al.*, 2004; Zhang, 2005] and further influence CO₂ sequestration in Arctic tundra ecosystems [Humphreys and Lafleur, 2011]. Thawing of the active layer and artificial drainage significantly decreased tundra tussock ecosystem C fluxes and global warming potential [Merbold *et al.*, 2009]. A mechanistic understanding of permafrost thaw and associated C dynamics will require simultaneous monitoring of the degree of permafrost thaw, moisture (snow, ice, and water) dynamics, and C fluxes and pools. Natali *et al.* [2011] suggest that soil saturation could inhibit growing season C emissions based on soil water content and respiration response to warming. However, it is usually infeasible to obtain all these data in a single study because of technical difficulty and labor intensity in these high-latitude ecosystems. Field experiments usually last over months or years that are much shorter than the timescale relevant to climate changes (e.g., decades or century); thus, a traditional warming experiment is essentially limited to simulate the realistic climate change scenario. Therefore, studies of permafrost thaw and subsequent C fluxes are relatively limited. Given the site-specific features, seasonal warming, and associated physical changes during permafrost thaw, it requires a comprehensive monitoring of warming-induced changes in ecosystem C processes, ground surface temperature and moisture dynamics simultaneously, which, however, is not trivial for field experimentalists. A process-based modeling approach, however, can help fill the gaps in the experimental observations because it enables us to quantify these highly relevant processes simultaneously and helps reveal the possible mechanisms that may explain the ecosystem responses to diverse range of warming trajectories [Luo, 2007].

In this study, we implemented the Community Atmosphere Biosphere Land Exchange model (CABLE v1.4 of Commonwealth Scientific and Industrial Research Organisation (CSIRO), Australia), which was calibrated based on observations at a tundra site in Alaska in order to explore permafrost thaw and subsequent ecosystem C exchange as affected by climate warming. This study simulated short- and long-term warming

(2°C) effects on permafrost thaw and ecosystem C fluxes under annual warming, winter warming, and summer warming, respectively. The short-term warming denotes stepwise warming (2°C) during 2007–2010, and long-term warming denotes gradual warming ($0.04^{\circ}\text{C yr}^{-1}$) during 2007–2056. Under stepwise warming, soil temperature, moisture, freezing and melting ice, growing season thaw depth, GPP, R_{eco} , and NEE are simulated; ALT and growing season length are derived based on the relevant simulations. We examined annual warming, winter warming, and summer warming effects on moisture dynamics (snow, ice, and water), growing season thaw depth, and ecosystem C fluxes. To predict long-term ecosystem response to warming, we conducted a 50 year long projection of annual warming, winter warming, and summer warming on GPP, R_{eco} , and NEE during 2007–2056. We hypothesized that (1) both stepwise and gradual warming shifted the ecosystem as a C sink to a source with the greatest effect by annual warming followed by winter warming and summer warming and (2) the pattern is driven by greater ecosystem respiration than plant growth. This study is expected to improve our understanding of ecosystem C cycle under annual and seasonal warming scenarios and the potential mechanisms that may regulate C exchange in this tundra ecosystem.

2. Materials and Methods

2.1. CABLE Model

The CABLE model has been developed from several predecessors in CSIRO as described in *Kowalczyk et al.* [2006] and *Wang et al.* [2011]. The first global land surface model (LSM) was developed at CSIRO, which used a single soil type, constant roughness length over land, and no vegetation. It was modified in the soil module to include six soil layers and three snow layers before coupling the LSM to the CSIRO Division of Atmospheric Research Limited Area Model. In the Soil Canopy Atmosphere Model (SCAM), the modeled canopy was located above the soil surface to allow for a more realistic aerodynamic coupling of land and atmosphere. SCAM also incorporated some novel treatment of canopy processes including turbulent transport over canopies and the representation of the interaction of the surface energy balance with plant physiology. *Wang and Leuning* [1998] developed a one-layer, two-leaf canopy model. The two-leaf model was named the CSIRO Biosphere Model (CBM). The first version of CABLE developed in 2003 combined all features of the predecessor LSMs. In particular, CABLE combines the two-leaf, sunshade canopy model from CBM, the model for surface roughness and aerodynamic resistance from SCAM, and the soil and snow model. CABLE is quite similar to Community Land Model (CLM) [*Oleson et al.*, 2010] and Organizing Carbon and Hydrology in Dynamic Ecosystems (ORCHIDEE) [*Krinner et al.*, 2005] in representing the range of biophysical processes for climate simulations. The performance of CABLE compares favorably with CLM and ORCHIDEE and other global LSMs in simulating surface fluxes of CO_2 , latent and sensible heat for different vegetation types [*Wang et al.*, 2007; *Abramowitz et al.*, 2008]. Some of major differences between CABLE, CLM, or ORCHIDEE lie in CABLE simulates radiative transfer in plant canopies based on the theory developed by *Goudriaan and van Laar* [1994] but CLM and ORCHIDEE based upon the two-stream approximation [*Sellers et al.*, 1986]; CABLE uses Ball-Berry-Leuning stomatal model [*Leuning*, 1995], whereas CLM and ORCHIDEE use the Ball-Berry stomatal model [*Ball et al.*, 1987].

The CABLE model simulates the exchanges of radiation, moisture, heat, and carbon at the land surface. It is provided with meteorological conditions (inputs) and, based on these, predicts fluxes (its outputs) such as latent heat flux, upward long-wave radiation, net ecosystem exchange of CO_2 , or drainage through deep soil. CABLE consists of five submodels: radiation, canopy micrometeorology, surface flux, soil and snow, and ecosystem respiration. The radiation submodel computes the net diffuse and direct beam radiation absorbed by each of two big leaves and by soil surface in the visible, near-infrared and thermal radiation, and the surface albedo for visible and near-infrared radiation. The canopy micrometeorology submodel computes canopy roughness length, zero plane in placement height and aerodynamic transfer resistance from the reference height or the height of the lowest layer in a climate model to within canopy air space or soil surface. The surface flux submodel computes fluxes of latent and sensible heat, and net canopy photosynthesis (see detail in Appendix A1). The soil and snow model computes temperature and moisture at different depths in soil, snow age, snow density and depth, and snow-covered surface albedo when snow is present (see detail in Appendix A2). The ecosystem respiration submodel computes the nonleaf plant tissue respiration, soil respiration, and net ecosystem CO_2 exchange (see detail in Appendix A1). The structure of CABLE model

codes is dictated by the relationship of inputs and outputs between different submodels. The CABLE model simulates energy budget at the ground surface and derives temperatures in multiple soil and snow layers based on rigorous accounting of radiation, latent heat, sensible heat at the interface of surface air through the surface snow, and soil layers to the boundary of permafrost soil. This model feature enables more accurate simulation of soil temperatures, which is a key for modeling tundra ecosystem C fluxes and permafrost thawing [Williams and Smith, 1989]. Other details in the model are referred to Kowalczyk *et al.* [2006] and Wang *et al.* [2011].

2.2. Site Characteristics

The Carbon in Permafrost Experimental Heating Research (CIPEHR) project was established in September 2008 at a moist acidic Arctic tundra site in Interior Alaska near Denali National Park [Schuur *et al.*, 2009; Natali *et al.*, 2011, 2012, 2014]. The site is situated on a relatively well-drained gentle northeast facing slope. Soils are Gelisols and are composed of an organic horizon, 0.45–0.65 m thick, above a cryoturbated mineral soil that is a mixture of glacial till and loess [Osterkamp *et al.*, 2009]. Underneath the top organic horizon, the ice-rich silt is about 500 cm deep followed by 23 m of gravel with boulders underlain by sand [Osterkamp *et al.*, 2009]. The active layer, which thaws annually during the growing season, is about 50–60 cm thick [Natali *et al.*, 2011] and is situated above a perennially frozen permafrost layer [van Everdingen, 2005; Grosse *et al.*, 2011]. Mean annual temperature (1976–2009) is about -1.0°C . The dominant vegetation at the site includes the tussock-forming sedge, *Eriophorum vaginatum*, and deciduous shrub, *Vaccinium uliginosum*, and nonvascular plant cover such as feather moss (i.e., *Pleurozium schreberi*) and *Sphagnum* spp., as well as several lichen species. The CIPEHR project was designed to passively increase winter and summer temperatures alone and in combination, to achieve air, soil, and permafrost warming to examine warming effects on permafrost thaw and associated C fluxes [Natali *et al.*, 2011]. At the site, the International Tundra Experiment-type open top chambers method is used to increase summer air and surface soil temperatures, and this method in addition to snow fences coupled with spring snow removal is applied to warm surface and deep soil temperatures in winter. The details of the experimental design can be found in Natali *et al.* [2011].

Here we briefly describe the methods measuring GPP, R_{eco} , NEE, and other C fluxes in the field but the full detail of these measurements can be found in Natali *et al.* [2011, 2012]. Aboveground biomass and net primary production were determined with a nondestructive point intercept method, coupled with allometric biomass equations developed for this site. Aboveground vascular plant net primary productivity (NPP) was estimated as the sum of the apical growth (leaves, stems, flowers, and fruits) and secondary growth for the current year [Natali *et al.*, 2011]. Net ecosystem exchange (NEE) and ecosystem respiration (R_{eco}) were measured using three automated CO_2 flux systems, each of which controlled eight flux chambers (60 cm \times 60 cm area) located within one experimental block (i.e., two snow fences). Autochamber measurements were supplemented with static chamber measurements in late spring (2–3 times per week), before the establishment of the automated system at all blocks. In late March and April, CO_2 fluxes were measured weekly in snow pits dug to the soil surface. Automated measurements were collected from each flux chamber every 1.5 h, beginning the first week of May through the last week of September, from 2009 through 2011. C balance during the growing season was estimated by gap filling flux measurements using response functions to environmental factors. To model wintertime R_{eco} , an exponential R_{eco} soil temperature equation was developed from winter flux data collected within the Environmental Measurements Laboratory watershed [Natali *et al.*, 2012]. Campbell Scientific (Logan, UT, USA) CR1000 data loggers recorded half-hourly soil temperature and moisture content since September 2008. Soil profile temperatures (5, 10, 20, and 40 cm) were measured using constantan-copper thermocouples. Thaw depth (TD) was measured weekly around the outside perimeter of each flux base using a metal depth probe. Monthly TD measurements were also taken inside the bases to determine potential summer warming effects on TD [Natali *et al.*, 2012].

2.3. Sensitivity Analysis

To employ the CABLE at a site level, a grid cell was chosen among 15238 cells in the model based on similar longitude and latitude as well as its soil and plant types to the site. A list of model parameters and their values in the original model (Table S1 in the supporting information) were kept unchanged when the model was run prior to the sensitivity analysis. We conducted model sensitivity analysis by varying a parameter value each time within its range while using the default values for other parameters (Table S1) then assessed

the sensitivities of the modeled soil temperature (5 and 40 cm) and snow temperature, CO₂ fluxes (GPP and R_{eco}), and volumetric water content (vol/vol). Sensitivity index (SI) is expressed as:

$$SI = \frac{|\log_{10}|\text{High output}|| - |\log_{10}|\text{Low output}||}{|\log_{10}|\text{High parameter}|| - |\log_{10}|\text{Low parameter}||} \quad (1)$$

SI less than 1 means that a magnitude change in the parameter results in less than a magnitude change in the output variable. If a parameter showed the highest sensitivity to certain variable, it was chosen as a tunable parameter in model calibration as described below.

2.4. Model Calibration and Validation

The CABLE model was calibrated against observations from the unmanipulated control plot from CiPEHR. The model was driven by the meteorological data collected from the site including air temperature, photosynthetic active radiation, precipitation, wind speed, and relative humidity. Data obtained from measurements were used to produce the input weather data required by the model. The model was first spun-up to steady state with the forcing data collected in 2006, 2006–2007, 2006–2008, and 2006–2009 based on a semianalytical solution method [Xia *et al.*, 2012]. The differences in steady state ecosystem carbon pool size among those runs were relatively small (10.8, 11.0, 11.1, and 10.9 kg C m⁻², respectively). Therefore, steady state pool sizes can be obtained during spin-up using 1 year meteorological forcing only. The model was thus spun-up to steady state with the forcing data collected in 2006 and was then used to simulate soil temperature, moisture, freezing and melting ice, GPP, and R_{eco} at a 3 h time step during 2007–2011. The observations at the control plot of the CiPEHR site were used to compare with the model simulation during 2007–2011. The model was calibrated using the measured soil temperatures at 5 cm and 40 cm depth in 2008 to 2010, soil volumetric water content (vol/vol) at the top 15 cm depth in 2009 and 2010, and GPP and R_{eco} during the growing seasons during 2009 to 2011. Based on sensitivity test results, we chose a set of sensitive parameters to target state variables (i.e., C fluxes, soil and snow temperatures, and soil water content) and adjusted the value of those parameters to minimize the squared difference between the modeled and observed values. Then, while maintaining the new parameter value, we conducted a similar procedure on another parameter until a better fit between simulation and observation was achieved. When a set of parameters and their new values were determined, we compared the model outputs with observations in order to evaluate the goodness of fit (see method below). After the calibration, model simulations were compared with independent data sets at the climate station nearby the CiPEHR site. The model performance was evaluated by the correlation coefficient (R^2) between simulation and observation.

We applied a number of statistical approaches to compare the model simulation and observation based on the methods in Hanson *et al.* [2004]. We first derived the linear regression slopes, intercepts, and determinant coefficient (R^2) as compared between observations and model simulations. To quantify the magnitude of bias and the mean deviation of simulations from the observation, we applied mean bias (MB) and mean absolute bias (MAB) calculated as follows in equations (2) and (3). The model was optimized by selecting the parameter values that lead to $|\text{MB}| < 0.5$ derived for GPP, R_{eco} , soil temperature, soil water content and thaw depth.

$$\text{MB} = \frac{\sum(\hat{y}_i - y_i)}{\sum(y_i)} \quad (2)$$

$$\text{MAB} = \frac{\sum|\hat{y}_i - y_i|}{n} \quad (3)$$

where \hat{y}_i denotes simulated values, y_i observed values, and n is the number of paired observation and simulation.

2.5. Thaw Depth

Thaw depth during the growing season identifies 0°C isotherm along the soil profile, i.e., soil depth where soil temperature was zero accompanied by greater temperature above the layer and lower temperature below it. As the observed permafrost thaw depth is about 10–20 cm in May and can be up to 60 cm in September, and a few centimeter increase of thaw depth can occur with experimental warming during the growing season [Natali *et al.*, 2011], a finer vertical resolution of simulated soil temperature profile within the soil was required to identify that variation of thaw depth. With its default setup, the CABLE model has six soil layers which bear the thickness from the top to bottom, 2.2, 5.8, 15.4, 40.9, 108.5, and 287.2 cm with a total

Table 1. Sensitivity Tests on Modeled GPP, R_{eco} , Soil Temperature at Six Layers (TS1–TS6), Snow Temperature at Three Snow Layers (TSN1–TSN3), and Volumetric Water Content (VWC, vol/vol)^a

Parameter	Units	Range	Value	GPP	R_{eco}	TS1	TS2	TS3	TS4	TS5	TS6	TSN1	TSN2	TSN3	VWC
<i>Soil Relevant</i>				<i>SI</i>											
Clay	-	0–1	0.33	0	0	1.1	1.1	1.7	1.0	0	0.5	0	0.1	0.2	0
Froot	-	0–1	0.125	0.1	0.1	0.1	0.1	0.2	1.0	0	1.5	0	0.1	0.7	0
Albsoil	-	0–0.9	0.237	0.1	0.1	0.9	0.7	0.5	0.2	0	0	0	0	0	0
Ssat	$m^3 m^{-3}$	0.35–0.5	0.45	0.7	0.4	0.8	0.8	0.7	0.5	0.4	0.4	0	0	0.2	0.9
<i>Plant Relevant</i>				<i>SI</i>											
v_{cmax}	$mol m^{-2} s^{-1}$	$5–150 \times 10^{-6}$	22×10^{-6}	0.3	0.1	0.06	0.06	0.06	0.06	0.08	0	0	0	0	0

^aSoil and plant relevant parameters that have been altered for model calibration are presented. Bold numbers denote sensitivity index (SI) more than 1 based on equation (1). Soil relevant parameters include soil clay content (clay), root fraction (froot) at the first soil layer, soil reflectance (albsoil), volumetric water content at soil saturation (ssat, vol/vol), maximum RuBP carboxylation rate top leaf (v_{cmax}).

depth of 460 cm. For this study, we modified the number of soil layers in the original model. Between the original first and second soil layers (2.2 cm and 5.8 cm thickness, respectively), we added 35 new soil layers with an even increase of thickness of 0.1 cm for each new layer from top to bottom. Each new soil layer was assumed to have the same thermal properties as the original layer at the same depth. We kept the original soil layer thickness including the original fifth and sixth layer thickness in order to include the thermal inertial of deep soil layers on temperature [Alexeev et al., 2007; Koven et al., 2009]. The new model has a total 41 layers in the soil thermal column, with a total depth of 600 cm. After the model was spun-up and reached equilibrium, we ran the simulations under each warming treatment. Then, we identified soil depth where the simulated mean daily soil temperature was $0.0 \pm 0.05^\circ C$ from May through September during 2007 to 2011.

2.6. Model Experiment

This study simulated short- and long-term warming ($2^\circ C$) effects on permafrost thaw and ecosystem C fluxes under annual warming, winter warming, and summer warming, respectively. The short-term warming denotes stepwise warming ($2^\circ C$) during 2007–2011, and long-term warming denotes gradual warming ($0.04^\circ C yr^{-1}$) during 2007–2056. Annual warming denotes ambient air temperature plus $2^\circ C$ during a whole year; winter warming denotes the same increase in air temperature only in January, February, March, April, October, November, and December; and summer warming denotes the same increase in air temperature in May, June, July, August, and September. For the simulations under the short-term stepwise warming, mean annual GPP, R_{eco} , and NEE were derived from the model simulations during 2007–2011. Net primary productivity (NPP), heterotrophic respiration (R_h) and autotrophic respiration (R_a) were also obtained from the model simulations. Based on soil temperature simulations, growing season 0° days was obtained by counting the number of days when soil temperature at 5 cm is equal to or more than $0^\circ C$ in each year during 2007–2011. Total soil water content in the soil profile (down to 15 cm) and the rate change in ALT under warming ($cm/^\circ C$) were also obtained during 2007–2011. To examine soil temperature increase on C balance, we conducted separate model simulations by rendering soil temperatures to be 0.5, 1.0, 1.5, and $2.0^\circ C$ higher than ambient condition. We also conducted a 50 year long model projection of gradual warming (annual warming, winter warming, and summer warming) on ecosystem C fluxes during 2007–2056. Based on the ambient temperature in 2006, the temperature forcing data during 2007 to 2056 represents a gradual air temperature increase ($0.04^\circ C yr^{-1}$) every year, to mimic a $2^\circ C$ temperature increase in this region in the first half of this century [ACIA, 2004; Intergovernmental Panel on Climate Change, 2007]. The control run represents a 50 year simulation with temperature each year equal to ambient temperature in 2006. Mean annual GPP, R_{eco} , NEE, and ALT were derived from the model simulations under the long-term gradual warming during 2007–2056.

3. Results

3.1. Sensitivity Analysis, Model Calibration, and Performance

Modeled soil and snow temperatures were most sensitive to changes in vertical distribution of root biomass in different soil layers and soil clay content ($SI > 1$, Table 1). GPP was most sensitive to maximum carboxylation rate ($SI = 0.3$), which was consistent with sensitivity analysis of the same and other ecosystem models [Baldocchi and Harley, 1995; Wohlfahrt et al., 2001; Lu et al., 2013].

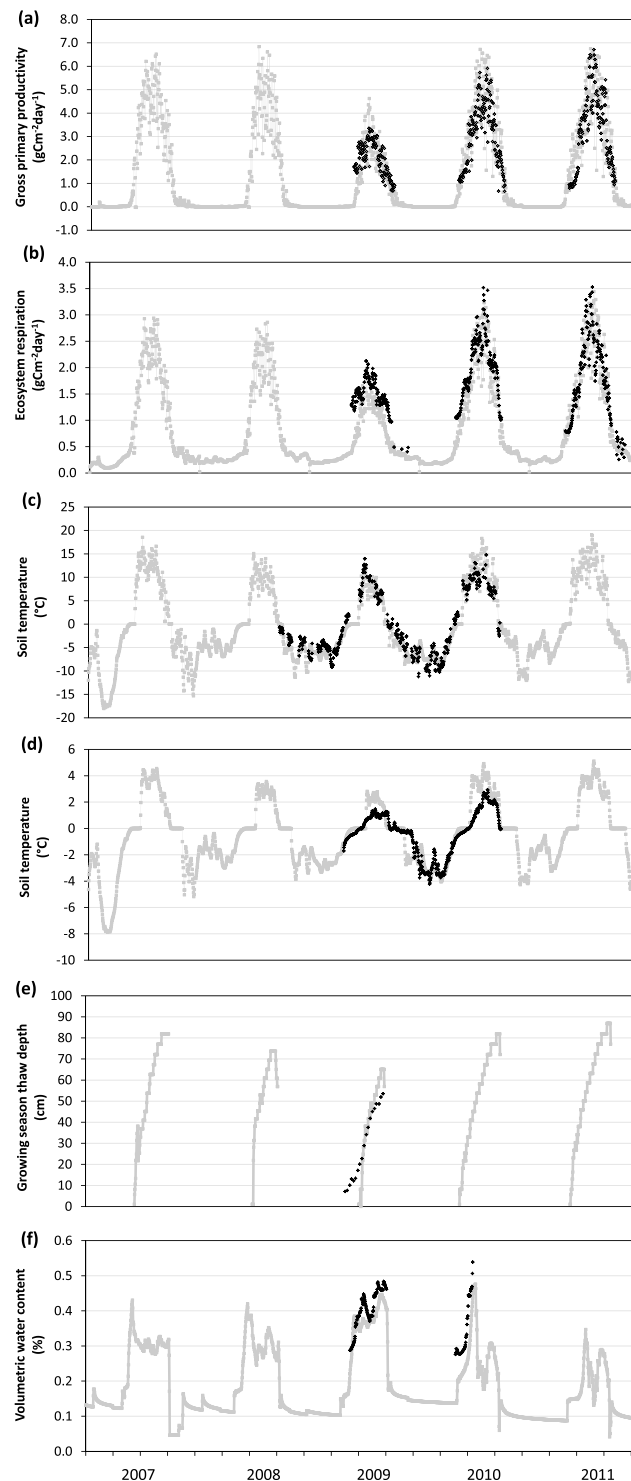


Figure 1. Simulated (grey) and observed (black) daily gross primary (a) productivity, (b) ecosystem respiration, soil temperature at (c) 5 cm and (d) 40 cm, (e) growing season thaw depth, and (f) soil volumetric water content integrated across the top 15 cm soil depth during 2007–2011.

followed by summer warming then winter warming both during the growing seasons and at the annual scale. The mean annual soil temperature increased by 0.8, 0.6, and 0.4°C (i.e., 5 cm) and by 0.3, 0.2, and 0.1°C (i.e., 40 cm) for annual warming, summer warming, and winter warming, respectively. The mean growing season

After calibration, the simulated GPP, R_{ecos} , soil temperature, thaw depth, and moisture content agreed well with observations during the growing season and annual scale (Figure 1 and Table 2). Soil temperature at 5 cm had smaller mean bias (MB) but greater mean absolute bias (MAB) than that at 40 cm (Table 2). Simulated soil temperature at 40 cm was slightly higher than the observed values during June to August. Simulated growing season thaw depth agreed well with observations and had a small MB and MAB, respectively. The agreement was good between the observed and simulated volumetric water content (VWC, vol/vol) of the top 15 cm depth. The simulated snow depth simulations agreed well with observations at the CiPEHR site in 2010 (Figure S1 in the supporting information) but was slightly thicker than the observed in 2009. The discrepancy may result from snow drifts caused by high winds at the site [Natali et al., 2011].

We evaluated the performance of the calibrated model using independent set of measurements (e.g., soil temperature and snow depth) from a site nearby the calibration site. The temporal pattern of simulated snow depth was consistent with the monitored snow depth at the local climate station during 2007–2011 ($R^2 > 0.60$, Figure S1). At 10 cm soil depth, simulated daily soil temperatures agreed well with the observations during 2007–2011 ($R^2 = 0.82$, Figure S2 in the supporting information). In comparison with independent GPP measurements in other similar sites in Arctic tundra region during the same time period [Belshe et al., 2013], our simulated plant growth is comparable with their observations and the model performance is thus acceptable for simulation of plant growth.

3.2. Effects of Stepwise Warming on Soil Temperature, Moisture, and Thaw Depth

Warming induced the greatest increase of soil temperature in annual warming,

Table 2. Model Performance for Gross Primary Productivity (GPP), Ecosystem Respiration (R_{eco}), Soil Temperature at 5 and 40 cm, Growing Season Thaw Depth, and Soil Volumetric Water Content Integrated Across the Top 15 cm Soil Depth (vol/vol)

Variable	Seasonality	Observation Versus Simulation Regression			Goodness-of-Fit	
		Slope	Intercept	R^2	MB	MAB
GPP	Annual	0.8812	0.4856	0.5655	0.0600	0.84
	Growing season	0.8756	1.0064	0.5728	0.09	0.44
R_{eco}	Annual	0.9952	-0.207	0.7161	-0.12	0.37
	Growing season	0.9133	0.046	0.6733	-0.11	0.42
Soil temperature (5 cm)	Annual	0.987	-0.2382	0.9345	-0.44	0.95
	Growing season	1.2466	-0.8876	0.6901	-0.50	1.30
Soil temperature (40 cm)	Annual	1.2298	0.456	0.8276	-0.80	0.55
	Growing season	1.2947	0.507	0.8427	-0.91	0.69
Soil moisture (0–15 cm)	Annual	0.9595	0.0254	0.7536	-0.11	0.05
	Growing season	0.9621	0.0321	0.7925	-0.09	0.08
Thaw depth	Growing season	1.7914	29.187	0.9602	0.06	0.21

soil temperature increased by 1.5, 1.0, and 0.6°C (i.e., 5 cm) and by 0.4, 0.3 and 0.2°C (i.e., 40 cm) for annual warming, summer warming, and winter warming, respectively. The mean wintertime soil temperature increased by 0.5, 0.4, and 0.2°C (i.e., 5 cm), and less than 0.1°C (i.e., 40 cm) for annual warming, summer warming, and winter warming, respectively. The mean growing season 0° days were 137, 134, 126, and 124 under annual warming, winter warming, summer warming, and ambient treatments, respectively.

Warming increased the amount of melting and freezing ice but decreased snow depth and soil water content in comparison to ambient condition (Figure 2a). Annual warming induced greater increase in melting and freezing ice than winter warming and summer warming, and annual warming and winter warming induced greater decreases in snow depth than summer warming, while there is no significant difference in soil water content between all three warming treatments (Figure 2b). Permafrost thaw depth increased under all warming

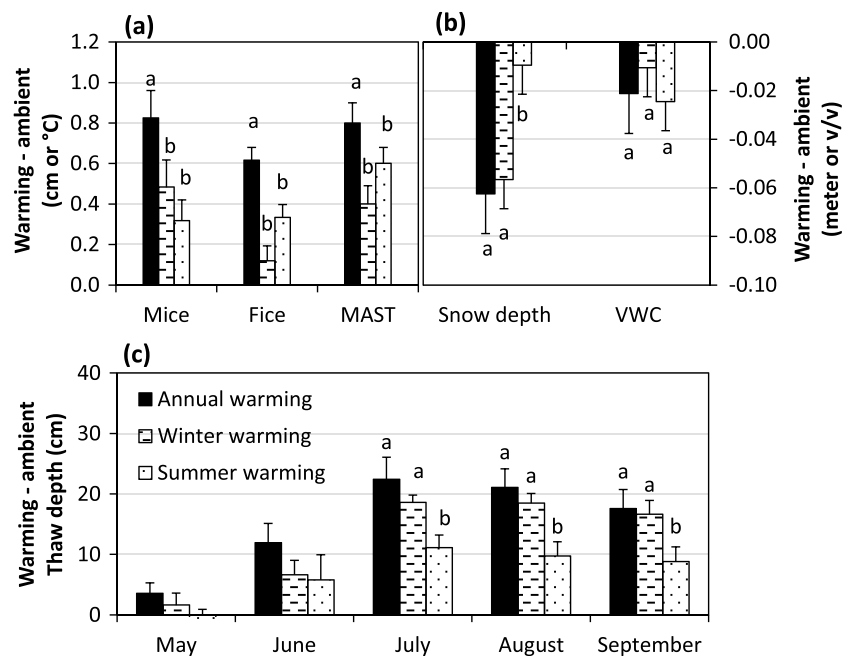


Figure 2. Mean (\pm SE) difference between warming and ambient treatments of (a) annual melting ice (Mice), freezing ice (Fice), and mean annual soil temperature (MAST, top 5 cm), (b) snow depth and volumetric water content (VWC, 0–15 cm), and (c) growing season thaw depth (cm). Annual warming, winter warming, and summer warming denote stepwise warming treatments.

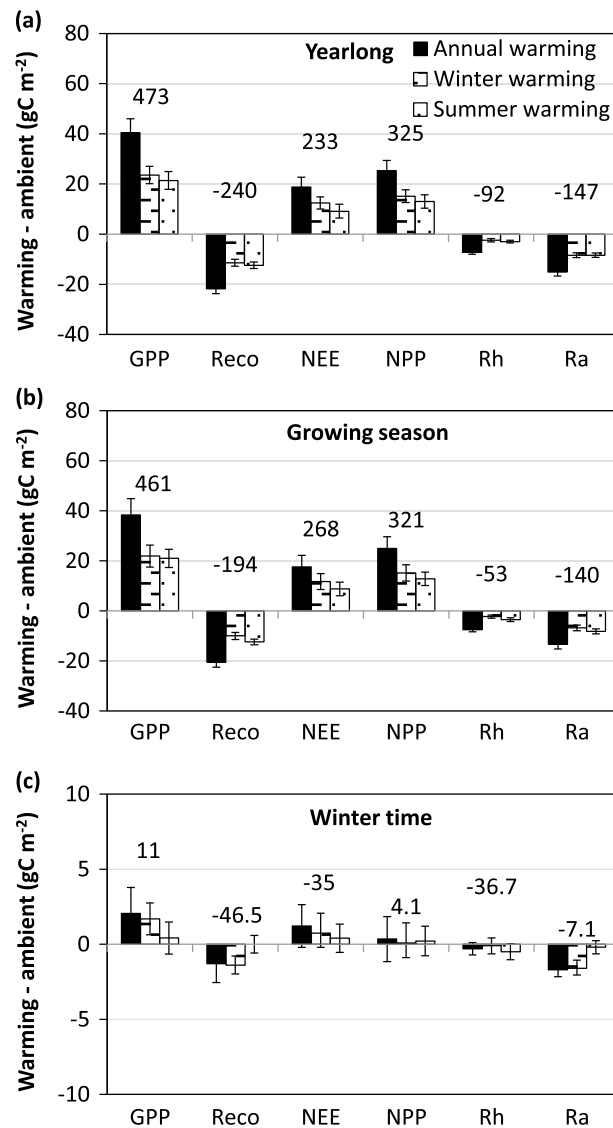


Figure 3. Simulated mean (\pm SE) of GPP, R_{eco} , NEE, NPP, R_h , and R_a during 2007–2011 under ambient (Con), stepwise annual warming, summer warming, and winter warming treatments scaled at (a) yearlong, (b) growing season, and (c) wintertime. Growing season denotes May–September, and wintertime denotes January–April and October–December.

significant correlations between growing season thaw depth and cumulative growing season GPP, R_{eco} , and NEE under all warming treatments but not under ambient treatment (Table 3). NPP, R_h , or R_a showed similar responses to warming in comparison with GPP and R_{eco} , respectively, and R_a showed consistently larger responses than R_h (Figures 3a–3c).

3.4. Long-Term Gradual Warming Effects on Ecosystem C Fluxes and Active Layer Thickness

Ecosystem C fluxes experienced a decadelong oscillation before each of them followed a monotonical change with time (Figures 4a–4c). In comparison to control simulation, annual warming, winter warming, and summer warming increased GPP by 11, 6, and 3% and increased R_{eco} by 13, 9, and 7% after 50 years, respectively; annual warming and winter warming increased NEE by 8 and 0.6% but summer warming decreased NEE by 1% after 50 years. Active layer thickness increased by 30, 15, and 12 cm under annual

treatments in comparison to ambient treatment during May to September (Figure 2c). In particular, annual warming and winter warming induced greater thaw depth than summer warming during July to September (Figure 2c). In comparison to ambient condition, annual warming, winter warming, and summer warming increase active layer thickness (ALT) by 8.8, 8.3, and 4.4 cm/°C, respectively.

3.3. Effects of Stepwise Warming on Ecosystem Carbon Fluxes

Annual GPP increased by 42, 23, and 21 g C m⁻² for annual warming, winter warming, and summer warming in comparison to ambient condition, respectively (Figure 3a). The response of GPP to warming during growing season followed a pattern similar to annual scale with a smaller magnitude (Figure 3b). Wintertime GPP increased by more than 3 g C m⁻² for annual warming and winter warming but only about 1 g C m⁻² for summer warming (Figure 3c). The respiratory C loss (i.e., R_{eco}) increased with all warming treatments and, in general, followed the same temporal change as GPP but with a smaller magnitude than GPP (Figures 3a–3c). All warming treatments, in general, induced positive NEE (i.e., ecosystem C accumulation or C sink) with the greatest C accretion by annual warming followed by winter warming and summer warming (Figures 3a–3c). In comparison to ambient treatment, annual warming, winter warming, and summer warming resulted in percentage increases by 12%, 6.1%, and 5.7% for annual GPP; 6.1%, 5.7%, and 4.5% for annual R_{eco} ; and 15%, 9.9%, and 5.8% for annual NEE, respectively. There were

Table 3. Pearson Product-Moment Correlation Coefficient and Significance Between Growing Season Active Layer Thickness (ALT) and Cumulative Growing Season Gross Primary Productivity (GPP), Ecosystem Respiration (R_{eco}), and Absolute NEE Under Ambient, Annual Warming (AW), Summer Warming (SW), and Winter Warming (WW) Treatments^a

ALT	GPP				R_{eco}				Absolute NEE			
	Ambient	Annual	SW	WW	Ambient	Annual	SW	WW	Ambient	Annual	SW	WW
Ambient	0.58				0.67				0.48			
Annual		0.92				0.93				0.88		
SW			0.89				0.89				0.87	
WW				0.94				0.94				0.88

^aData are paired based on year during 2007–2011 ($N=5$). Bold numbers denote significant correlation coefficients at p value < 0.05 .

warming, winter warming, and summer warming in comparison to control run after 50 year long gradual warming (Figure 4d).

4. Discussion

4.1. Warming Increased Permafrost Thaw but Enhanced Ecosystem C Accretion

Permafrost thaw subject to climate warming can liberate formerly frozen C, which is then released to atmosphere [Davidson et al., 2006; Schuur et al., 2008, 2009; Tarnocai et al., 2009; Grosse et al., 2011; Koven et al., 2011; van Huissteden et al., 2011; Harden et al., 2012; Knoblauch et al., 2013; Pries et al., 2013; Schuur et al., 2013]. This suggests that enhanced permafrost thawing from warming potentially leads to more C loss and may shift the ecosystem C balance toward a weaker sink or a source [Osterkamp and Jorgenson, 2006; Osterkamp, 2007; Schuur et al., 2008]. However, this study suggests that the increased permafrost thaw from

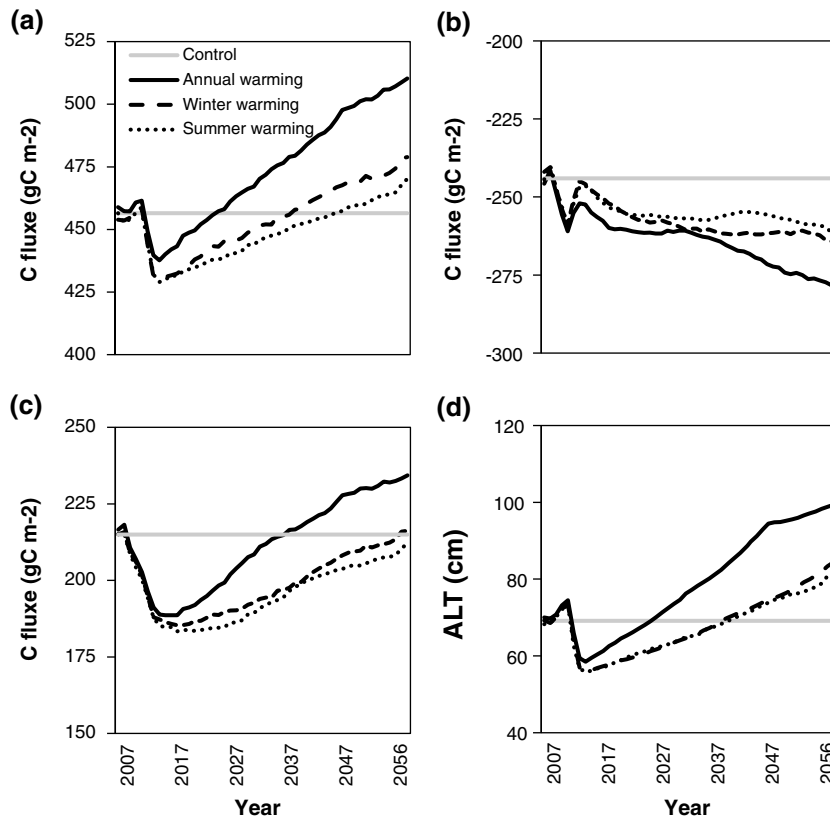


Figure 4. Simulated 50 year long gradual warming (0.04°C yr⁻¹) effects on (a) GPP, (b) R_{eco} , and (c) NEE and (d) active layer thickness (ALT) under control (grey), annual warming (solid), winter warming (dashed), and summer warming (dotted) during 2007–2056.

warming may not necessarily lead to more C loss from ecosystem. On the contrary, warming enhances ecosystem C accretion over short-term stepwise warming or long-term gradual warming scenarios because of greater C input via plant growth than C loss via respiration.

This disproportional change in soil respiration might be due to inhibiting effect of soil saturation on respiratory C loss [Natali *et al.*, 2011]. However, we found insignificant difference in soil water content between warming and ambient condition during the growing season (Figure 2b). In addition, the earlier thawing increased the entire growing season thaw depth and active layer thickness, which is consistent with former studies [Hinkel *et al.*, 1997; Waelbroeck *et al.*, 1997; Anisimov *et al.*, 2002; Hinkel and Nelson, 2003; Frauenfeld *et al.*, 2004; Zimov *et al.*, 2006a; Beer *et al.*, 2007; Khvorostyanov *et al.*, 2008a; Smith *et al.*, 2009; Burke *et al.*, 2012; von Deimling *et al.*, 2012]. However, this warming effect appears to have extended growing season 0° days (i.e., >137 versus 134).

The warming-induced changes of both soil respiration and ecosystem C balance depend on the response of soil temperature change to air warming. The high sensitivities of simulated soil temperature in response to root biomass and clay content are consistent with former findings that these two properties determined soil heat conductivity and capacity, and soil water dynamics, thus regulated the energy penetrating into the soil and also the energy emission from the ground surface [Stieglitz *et al.*, 2003; Langer *et al.*, 2011]. We specifically analyzed stepwise warming effects on soil temperature increase and ecosystem C balance in 2009 when observations are available. The simulated soil temperature increase is about 0.1°C while the observed soil temperature increase is about 1.5°C during the wintertime at the top 40 cm soil profile [Natali *et al.*, 2011]. Under the simulated temperature increase (i.e., 0.1°C), wintertime ecosystem respiration increased by 4.9% under winter warming than ambient condition (i.e., ambient = 59.7 g C m⁻², winter warming = 62.7 g C m⁻²), while the observed wintertime respiration increased by 56% (i.e., ambient = 76 g C m⁻², winter warming = 119 g C m⁻²). Based on temperature sensitivity of respiration ($Q_{10} = 2$) and the mean wintertime temperature (-5°C), this difference of temperature increase can induce more than 10 times more percentage increase in wintertime respiration as observed than as simulated. This explained the difference of 4.9% and 56% in wintertime respiration as elaborated above. The much lower temperature increase in soil also explained the smaller responses of heterotrophic respiration than autotrophic respiration.

As a key variable in permafrost environment, increasing soil temperature under climate warming can accelerate snow disappearance, degrade snow insulation, increase belowground microbial activities, and alter ecosystem C balance [Stieglitz *et al.*, 2003; Dorrepaal *et al.*, 2004; Zhang, 2005; Langer *et al.*, 2011; O'Donnell *et al.*, 2011; Li *et al.*, 2012, 2013]. In a separate simulation, a greater soil temperature (i.e., 1.5°C as observed in the field warming experiment) led to a similar percentage increase in wintertime respiration. In comparison to simulated plant growth, the tundra ecosystem can change from net C sink to net C source to atmosphere CO₂ (i.e., 12.6 g C m⁻² yr⁻¹ gain to 18.1 g C m⁻² yr⁻¹ loss). This suggests that under climate warming, the degree of soil warming regulated the extent of respiratory C loss and subsequent ecosystem C balance. This is corroborated by the significant correlations between thaw depth and C fluxes only under the warming treatments (Table 3).

Long-term gradual warming also induced large increases in permafrost thaw depth and active layer thickness (Figure 4d). Unlike short-term stepwise warming, permafrost thaw was enhanced with the largest magnitude by annual warming and similar increases in permafrost thaw by winter warming and summer warming. The gradual warming scenario experienced 50 times lower temperature increase each year than stepwise warming (0.04°C versus 2.0°C). Soil temperature is a key control of soil water and ice content which can directly alter thermal properties across the soil profile, which in turn exert strong feedback on soil temperature change subsequently. As C flux is highly sensitive to soil temperature (i.e., microbial decomposition and uptake and nutrient mineralization and turnover), the major difference in soil temperature increase thus can lead to substantially contrasting dynamics of C flux under step and gradual warming scenarios. Given the fact that climate warming most likely will occur gradually, the ecosystem C fluxes and permafrost thaw under long-term simulation in this study may exhibit a more realistic pathway and consequence under future warming in this region and other areas alike.

4.2. Annual Warming Resulted in Larger Effect on Ecosystem C Fluxes Than Seasonal Warming

Annual warming induced the greatest increases in C fluxes, C accretion, permafrost thaw depth, and greatest decreases in snow depth and the amount of ice melting and freezing under both stepwise and gradual warming scenarios. Winter warming induced greater C accretion, melting ice, thaw depth under stepwise

warming, and larger changes in C fluxes under long-term gradual warming than summer warming. In spite of larger C accretion under stepwise warming, winter warming only induced a relatively minor increase in the amount of C accretion under long-term gradual warming. Summer warming, however, reduced the C accretion. These data suggest that even though winter warming is predicted to be more pronounced this century, its effect on ecosystem C balance is likely to further increase ecosystem C uptake. If the simulated soil temperature were greater, our simulations do reveal winter warming would reverse the ecosystem from a net C sink to a C source at this site. Under either short-term stepwise warming or long-term gradual warming, summer warming appeared to have minimal effect on ecosystem C balance. This indicates that future summer temperature increase may have equivalent effect on C input to and C loss from the tundra ecosystem, thus inducing very limited effect on ecosystem C budget.

5. Conclusion

Some evidence showed that terrestrial ecosystems (e.g., tundra) might be a weak C sink rather than a C source under global climate warming [Shaver *et al.*, 2000; Smith *et al.*, 2004; Zimov *et al.*, 2006b; Hollingsworth *et al.*, 2008; McGuire *et al.*, 2009; Zhuang *et al.*, 2010; Elmendorf *et al.*, 2012; Lu *et al.*, 2012], but other evidence points in the opposite direction [Belshe *et al.*, 2013; Natali *et al.*, 2014]. Our short-term and 50 year long projection showed that annual warming and winter warming increase the C sink strength rather than decrease C. Our study support that the tundra ecosystem will remain as a weak C sink at least in the first half of this century.

This study revealed that both stepwise and gradual warming enhanced ecosystem C accretion because the increase in photosynthetic C uptake is greater than the increase in ecosystem respiration under warming. Furthermore, the contrasting response of respiration and plant growth is attributed to much lower soil temperature increase than air warming, and reverses if warmer winter temperatures were simulated. This finding has important implications for prediction of future climate changes in tundra region. It is critical to reconcile the discrepancy between modeled and observed increases in soil temperature because much lower soil temperature increase as modeled predicts ecosystem C accretion, whereas modeled soil temperature increase as high as the field experiment resulted in pronounced ecosystem C loss. As a key variable in permafrost environment, soil temperature should be measured under simulated air warming in the field. However, it remains uncertain whether soil temperature should be increased directly in the field as it might not represent the realistic response of soil temperature to future surface air warming. This gap between model and experiment also implied that an improvement of simulation of snow, ice, and water dynamics under air warming will essentially improve our ability in predicting the future ecosystem C balance and C cycle-climate feedback.

Appendix A: Model Description

Warming of climate can affect many carbon processes, as both photosynthesis and respiration are strongly dependent on air or soil temperature and moisture. Warming can also increase water loss from soil or snow sublimation and accelerating snowmelt in spring time, hence soil water and temperature dynamics. Kowalczyk *et al.* [2006] and Wang *et al.* [2010, 2011] have provided description of all key components of CABLE, including the model of soil temperature and moisture. Here we include a brief description of key carbon processes and the snow model and how processes in those two components vary with temperature.

A1. Carbon Processes

A1.1. Gross Primary Productivity

GPP in $\text{g C m}^{-2} \text{d}^{-1}$ is calculated as the gross photosynthesis using the two-leaf model of Wang and Leuning [1998]. That is,

$$\text{GPP} = (1 - \Gamma^*/C_i)V_c(v_{c\max}, j_{\max}, K_c, K_o, C_i, Q, L) \quad (\text{A1})$$

where Γ is the CO_2 compensation point in the absence of day respiration in ppmv and is a function of leaf temperature [Leuning, 1990], C_i is intercellular CO_2 concentration in ppmv, V_c is carboxylation rate and depends on maximum carboxylation rate ($v_{c\max}$), maximum rate of potential electron transport (j_{\max}), Michaelis-Menton constant for CO_2 carboxylation (K_c) or for O_2 oxygenation (K_o), C_i , absorbed photosynthetically active radiation (Q), and canopy leaf area index (L). Parameters $v_{c\max}$, j_{\max} , K_c , and K_o all vary with leaf temperature [Leuning, 1990].

A1.2. Net Canopy Photosynthesis

In the surface flux submodel, canopy photosynthesis and transpiration is coupled through stomatal conductance that is modeled using the following model [Ball et al., 1987; Leuning, 1990]:

$$G_{s,i} = G_{0,i} + \frac{a_1 f_{\text{wsoil}} A_{c,i}}{(C_{s,i} - \Gamma)(1 + D_{s,i}/D_0)} \quad (\text{A2})$$

Where $G_{0,i}$ is the residual or cuticular conductance in $\text{mol m}^{-2} \text{s}^{-1}$, $D_{s,i}$, $C_{s,i}$, and $A_{c,i}$ are the water vapor pressure deficit at the leaf surface (Pa), CO_2 concentration at the leaf surface in mol mol^{-1} , and net photosynthesis of leaf i in $\text{mol m}^{-2} \text{s}^{-1}$, respectively. Γ is the CO_2 concentration point of photosynthesis in mol m^{-1} and is a function of canopy temperature (T_c) [Leuning, 1990]; a_1 and D_0 are two model parameters ($a = 4$ for C4 plant and $= 9$ for C3 plants, $D_0 = 1500$ Pa); f_{wsoil} is the influence of soil water limitation on stomatal conductance and is calculated as

$$f_{\text{wsoil}} = \beta_v \sum_m f_{\text{root},m} \frac{\theta_m - \theta_{\text{wilt}}}{\theta_{\text{fc}} - \theta_{\text{wilt}}} \quad (\text{A3})$$

where β_v is the model parameter and $f_{\text{root},m}$ is the fraction of root mass in soil layer m ; θ_m is the volumetric soil water content of soil layer m and θ_{fc} and θ_{wilt} are the volumetric soil water contents at field capacity and wilting point, respectively.

Details for the calculation of plant maintenance and growth respirations have been provided by Zhang et al. [2013]. Plant maintenance respiration in CABLE is calculated as the sum of maintenance respiration rates of leaf, wood, and root, and which also vary with plant tissue temperature. Heterotrophic respiration depends on sizes of different carbon pools in the soil and their turnover rates. The turnover rate of each soil carbon pool is a function of soil temperature and moisture [Wang et al., 2010]; therefore, heterotrophic respiration is also dependent on soil temperature and moisture in the rooting zone.

The ecosystem respiration submodel calculates the respiration of wood, root, and soil. They are calculated as

$$R_{\text{wood}} = x_p r_{\text{wood}} f_1(T_a) C_{\text{wood}} \quad (\text{A4})$$

$$R_{\text{root}} = x_p r_{\text{root}} f_1(T_a) C_{\text{root}} \quad (\text{A5})$$

$$R_{\text{soil}} = x_p r_{\text{soil}} f_2(\bar{T}_s, \bar{\theta}_s) \quad (\text{A6})$$

where C_{wood} and C_{root} are the amounts of carbon in wood and roots (g C m^{-2}), respectively; r_{wood} , r_{root} , and r_{soil} are the respiration rates of wood, root, and soil (at $T_a = 20^\circ\text{C}$ for wood or $\bar{T}_s = 285$ K for root and soil) in $\mu\text{mol m}^{-2} \text{s}^{-1} (\text{g C})^{-1}$ for wood and root, and in $\mu\text{mol m}^{-2} \text{s}^{-1}$ for soil; they are biome-specific model parameters [Kowalczyk et al., 2006]. \bar{T}_s is the root mass weighted mean of soil mean temperature (K), and $\bar{\theta}_s$ is the root mass weighted mean of soil water content and is calculated as

$$\bar{\theta}_s = \sum_m f_{\text{root},m} \frac{\theta_m - \theta_{\text{wilt}}}{\theta_{\text{fc}} - \theta_{\text{wilt}}} \quad (\text{A7})$$

where $f_{\text{root},m}$ is the fraction of root mass in soil layer m and θ_m is the volumetric soil water content of soil layer m ; θ_{fc} and θ_{wilt} are the volumetric soil water contents at field capacity and wilting point, respectively. The functions f_1 and f_2 are calculated as

$$f_1(T) = (3.22 - 0.046T)^{0.1(T-20)} \quad (\text{A8})$$

$$f_2(\bar{T}_s, \bar{\theta}_s) = b_1 \exp\left((b_2 + b_3 \bar{\theta}_s) \left(\frac{1}{\bar{T}_{\text{avg}} - T_{s0}} - \frac{1}{\bar{T}_s - T_{s0}}\right)\right) \frac{\bar{\theta}_s}{\bar{\theta}_s - \theta_{s0}} \quad (\text{A9})$$

The function f_1 is based on the work of Tjoelker et al. [2001], and f_2 is based on the work of Reichstein et al. [2002], where b_1 is a biome-dependent model parameter ($\mu\text{mol m}^{-2} \text{s}^{-1}$) and the empirical constants b_2 , b_3 , T_{s0} , and θ_{s0} are equal to 52.4 (K), 285 (K), 227.2 (K), and 0.16, respectively Reichstein et al. [2002]. \bar{T}_{avg} is the annual mean soil temperature (K) and is assumed to be equal to the temperature of the deepest soil layer ($T_{s,6}$).

The net ecosystem exchange of CO₂, NEE, is then calculated as

$$NEE = A_C - R_{\text{wood}} - R_{\text{root}} - R_{\text{soil}} \quad (\text{A10})$$

Inputs to this submodel are temperature of the air within the canopy (T_a), root mass weighted mean temperature and moisture of the soil ($\bar{T}_s, \bar{\theta}_s$), and the amount of carbon in root (C_{root} in g C m⁻²) and wood (C_{wood} in g C m⁻²); and the output of this submodel is NEE.

Net ecosystem exchange (NEE) in g C m⁻² d⁻¹ CABLE is calculated as the difference between gross photosynthesis (GPP) and the sum of autotrophic (R_a) and heterotrophic (R_h) respiration. Autotrophic respiration is further separated into maintenance (R_m) and growth (R_g) respiration.

$$NEE = \text{GPP} - R_m - R_g - R_h \quad (\text{A11})$$

A2. Snow Model

Snow covers tundra at northern high latitudes for about 7–8 months within a year. Snow cover increases surface albedo, thereby reduces the available energy at the land surface. Snow cover also prevents excessive soil heat loss to the atmosphere and allows the temperature of the underlying soil to remain warmer than the ambient air above. The insulating properties of the snow are due to its low thermal conductivity, which for new snow is roughly an order of magnitude lower than that of the soil. A typical temperature profile throughout the early winter snowpack has a strong vertical gradient immediately below the surface and a weak gradient close to the ground [Gray and Male, 1981].

A simple one layer version of snow model is used in CABLE for this study as described in Gordon *et al.* [2002]. Snow models are sensitive to snow-rain criterion as described by Loth *et al.* [1993] and Yang *et al.* [1997]. The simple snow-rain threshold of 0°C is used only in the off-line version of CABLE; the online implementation uses fraction of liquid/solid precipitation computed by the cloud liquid water parameterization included in the host atmospheric model. The prognostic state variables for describing the snow cover mass and heat content are the following: snow mass M_{sn} in water equivalent, snow density (ρ_{sn}) and temperature (T_{sn}). These variables are updated every time step (1 h for this study).

Change in snow mass is calculated based on mass balance. That is,

$$\frac{dM_{\text{sn}}}{dt} = P_s + P_l - E_{\text{sn}} - V \quad (\text{A12})$$

where P_s is snowfall rate, P_l is rainfall rate, E_{sn} is snow sublimation rate, and V is the rate of snow melting. All these variables have a unit of kg m⁻² s⁻¹.

Snow density (ρ_{sn}) affects snow temperature through its effects on snow thermal conductivity and snow albedo. The density of fresh snow is 100 kg m⁻³ and may increase to 450 kg m⁻³ as a result of settling and compaction. Their effect on snow density are calculated as

$$\frac{1}{\rho_{\text{sn}}} \frac{\partial \rho_{\text{sn}}}{\partial t} = f_3(T_{\text{sn}}, \rho_{\text{sn}}) + f_4(M_{\text{sn}}, \rho_{\text{sn}}) \quad (\text{A13})$$

where functions f_3 and f_4 represents the effect of settling and compaction on snow density, respectively [Gordon *et al.*, 2002].

Following the calculation of snow densification, the thickness of the adjusted layer is calculated by accounting for the new snowfall, snowmelt, sublimation, and densification. Mass and heat content is redistributed, and heat conduction within the snow layer is calculated by solving the following equation numerically. That is,

$$\rho_{\text{sn}} c_{\text{sn}} \frac{\partial T_{\text{sn}}}{\partial t} = \frac{\partial}{\partial z} \left(\kappa_{\text{sn}} \frac{\partial T_{\text{sn}}}{\partial z} \right) \quad (\text{A14})$$

where c_{sn} and κ_{sn} are specific heat capacity (taken as 2095 J kg⁻¹ K⁻¹) and thermal conductivity in W m⁻¹ K⁻¹

of the snow layer and κ_{sn} is a function of snow density [Anderson, 1976]. As snow ages, its density increases so does its thermal conductivity.

At the bottom of the snowpack boundary the energy balance is influenced by the ground heat flux through the soil surface. At the top, the energy balance of the snow cover is influenced by the net heat flux at the surface as follows:

$$(1 - \alpha_{sn})S + L_s - \varepsilon_{sn}\sigma T_{sn}^4 + Q_r - H_{sn} - \lambda E_{sn} - G_{sn} = 0 \quad (A15)$$

where α_{sn} is a snow albedo, S is the incoming short wave in $W m^{-2}$, and L_s is the incoming long-wave radiation in $W m^{-2}$; ε_{sn} is the emissivity of the snow, and Q_r is the energy input due to rain in $W m^{-2}$. As liquid rainfall freezes in the first layer, it releases latent heat on contact with the snow. H_{sn} and λE_{sn} represent sensible heat and latent heat fluxes from snow.

Snow can modify the surface energy balance by changing the surface radiation balance. The total surface albedo of a land with partial or complete snow cover, α_s , is a function of canopy albedo, snow albedo, and bare ground albedo. The albedo of snow, α_{sn} , is a function of snow age (τ_{sn}), zenith angle of the sun (θ), and albedo of fresh snow which is 0.95 for visible radiation and 0.65 for near-infrared radiation.

Snow age (τ_{sn}) as a prognostic variable in CABLE is a nondimensional variable. Its change between two successive time steps in CABLE is calculated as

$$\Delta\tau_{sn} = f_5(T_{sn}, M_{sn})\Delta t \quad (A16)$$

where Δt is the time step of model integration (= 3600 s in this study). See Dickinson *et al.* [1993] for further details about function f_5 .

We also assume that a snowfall of 0.01 m in liquid water equivalent will restore the snow age to that of fresh snow. To account for this effect, the snow age at time $t + 1$ is calculated as

$$\tau_{sn}(t + 1) = (\tau_{sn}(t) + \Delta\tau_{sn})(1 - P_{sn}) \quad (A17)$$

Acknowledgments

We thank two anonymous reviewers for their insightful and valuable comments. This study was financially supported by the U.S. National Science Foundation (NSF) grant DBI 0850290, EPS 0919466, DEB 0743778, DEB 0840964, EF 1137293, and the DOE grant DE-SC0006982. Part of the model runs was performed at the Supercomputing Center for Education and Research (OSKER), University of Oklahoma. The authors have no conflict of interest to declare.

References

- Abramowitz, G., R. Leuning, M. Clark, and A. Pitman (2008), Evaluating the performance of Land Surface Models, *J. Climate*, *21*, 5468–5481.
- Arctic Climate Impact Assessment (2004), *Impacts of a Warming Arctic*, Cambridge Univ. Press, Cambridge.
- Alexeev, V. A., D. J. Nicolsky, V. E. Romanovsky, and D. M. Lawrence (2007), An evaluation of deep soil configurations in the CLM3 for improved representation of permafrost, *Geophys. Res. Lett.*, *34*, L09502, doi:10.1029/2007GL029536.
- Anderson, E. A. (1976), A point energy and mass balance model of a snow cover, 150 pp., Office of Hydrology, National Weather Service.
- Anisimov, O. A., N. I. Shiklomanov, and F. E. Nelson (1997), Global warming and active-layer thickness: Results from transient general circulation models, *Global Planet. Change*, *15*, 61–77.
- Anisimov, O. A., N. I. Shiklomanov, and F. E. Nelson (2002), Variability of seasonal thaw depth in permafrost regions: A stochastic modeling approach, *Ecol. Model.*, *153*, 217–227.
- Baldocchi, D. D., and P. C. Harley (1995), Scaling carbon dioxide and water vapour exchange from leaf to canopy in a deciduous forest. II. Model testing and application, *Plant Cell Environ.*, *18*, 1157–1173.
- Ball, J. T., I. E. Woodrow, and J. A. Berry (1987), A model predicting stomatal conductance and its contribution to the control of photosynthesis under different environmental conditions, in *Progress in Photosynthesis Research*, edited by I. Biggens, pp. 221–224, Martinus-Nijhoff, Dordrecht, Netherlands.
- Beer, C., W. Lucht, D. Gerten, K. Thonicke, and C. Schmullius (2007), Effects of soil freezing and thawing on vegetation carbon density in Siberia: A modeling analysis with the Lund-Potsdam-Jena Dynamic Global Vegetation Model (LPJ-DGVM), *Global Biogeochem. Cycles*, *21*, B1012, doi:10.1029/2006GB002760.
- Belshe, E. F., E. A. G. Schuur, B. M. Bolker, and R. Bracho (2012), Incorporating spatial heterogeneity created by permafrost thaw into a landscape carbon estimate, *J. Geophys. Res.*, *117*, G01026, doi:10.1029/2011JG001836.
- Belshe, E. F., E. A. G. Schuur, and B. M. Bolker (2013), Tundra ecosystems observed to be CO₂ sources due to differential amplification of the carbon cycle, *Ecol. Lett.*, *16*, 1307–1315.
- Brzostek, E. R., and A. C. Finzi (2012), Seasonal variation in the temperature sensitivity of proteolytic enzyme activity in temperate forest soils, *J. Geophys. Res.*, *117*, G01018, doi:10.1029/2011JG001688.
- Burke, E. J., I. P. Hartley, and C. D. Jones (2012), Uncertainties in the global temperature change caused by carbon release from permafrost thawing, *Cryosphere*, *6*, 1063–1076.
- Chapin, F. S., et al. (2000), Arctic and boreal ecosystems of western North America as components of the climate system, *Glob. Chang. Biol.*, *6*, 211–223.
- Dankers, R., E. J. Burke, and J. Price (2011), Simulation of permafrost and seasonal thaw depth in the JULES land surface scheme, *Cryosphere*, *5*, 773–790.
- Davidson, E. A., I. A. Janssens, and Y. Q. Luo (2006), On the variability of respiration in terrestrial ecosystems: Moving beyond Q(10), *Glob. Chang. Biol.*, *12*, 154–164.
- Dickinson, R. E., A. Henderson-Sellers, and P. J. Kennedy (1993), Biosphere-Atmosphere Transfer Scheme (BATS) version 1e as coupled to the NCAR Community Climate Model. NCAR Technical Note NCAR/TN-387+STR, 72 pp.

- Dorrepaal, E., R. Aerts, J. H. C. Cornelissen, T. V. Callaghan, and R. S. P. van Logtestijn (2004), Summer warming and increased winter snow cover affect Sphagnum fuscum growth, structure and production in a sub-arctic bog, *Glob. Chang. Biol.*, *10*, 93–104.
- Elmendorf, S. C., et al. (2012), Plot-scale evidence of tundra vegetation change and links to recent summer warming, *Nat. Clim. Change*, *2*, 453–457.
- Frauenfeld, O. W., T. J. Zhang, R. G. Barry, and D. Gilichinsky (2004), Interdecadal changes in seasonal freeze and thaw depths in Russia, *J. Geophys. Res.*, *109*, D05101, doi:10.1029/2003JD004245.
- Gordon, H. B., et al. (2002), The CSIRO Mk3 Climate System Model, CSIRO Atmospheric Research technical paper 60. [Available at http://www.cmar.csiro.au/e-print/open/gordon_2002a.pdf.]
- Goudriaan, J., and H. H. van Laar (1994), *Modeling Potential Crop Growth Processes*, Kluwer Acad., Dordrecht, Netherlands.
- Gray, D. M., and D. H. Male (1981), *Handbook of Snow: Principles, Processes, Management and Use*, Pergamon Press, Toronto.
- Grogan, P., and F. S. Chapin (1999), Arctic soil respiration: Effects of climate and vegetation depend on season, *Ecosystems*, *2*, 451–459.
- Grosse, G., et al. (2011), Vulnerability of high-latitude soil organic carbon in North America to disturbance, *J. Geophys. Res.*, *116*, G00K06, doi:10.1029/2010JG001507.
- Hanson, P. J., et al. (2004), Oak forest carbon and water simulations: Model intercomparisons and evaluations against independent data, *Ecol. Monograph*, *74*, 443–489.
- Harden, J. W., et al. (2012), Field information links permafrost carbon to physical vulnerabilities of thawing, *Geophys. Res. Lett.*, *39*, L15704, doi:10.1029/2012GL051958.
- Hayes, D. J., A. D. McGuire, D. W. Kicklighter, K. R. Gurney, T. J. Burnside, and J. M. Melillo (2011), Is the northern high-latitude land-based CO₂ sink weakening?, *Global Biogeochem. Cycles*, *25*, GB3018, doi:10.1029/2010GB003813.
- Hinkel, K. M., and F. E. Nelson (2003), Spatial and temporal patterns of active layer thickness at Circumpolar Active Layer Monitoring (CALM) sites in northern Alaska, 1995–2000, *J. Geophys. Res.*, *108*(D2), 8168, doi:10.1029/2001JD000927.
- Hinkel, K. M., S. I. Outcalt, and A. E. Taylor (1997), Seasonal patterns of coupled flow in the active layer at three sites in northwest North America, *Can. J. Earth Sci.*, *34*, 667–678.
- Hollingsworth, T. N., E. A. G. Schuur, F. S. Chapin, and M. D. Walker (2008), Plant community composition as a predictor of regional soil carbon storage in Alaskan boreal black spruce ecosystems, *Ecosystems*, *11*, 629–642.
- Humphreys, E. R., and P. M. Lafleur (2011), Does earlier snowmelt lead to greater CO₂ sequestration in two low Arctic tundra ecosystems?, *Geophys. Res. Lett.*, *38*, L09703, doi:10.1029/2011GL047339.
- Intergovernmental Panel on Climate Change (2007), Climate change 2007: The physical science basis. Working group I contribution to the Intergovernmental Panel on Climate Change Fourth Assessment Report. [Available at <http://www.ipcc.ch/>]
- Khvorostyanov, D. V., P. Ciais, G. Krinner, and S. A. Zimov (2008a), Vulnerability of east Siberia's frozen carbon stores to future warming, *Geophys. Res. Lett.*, *35*, L10703, doi:10.1029/2008GL033639.
- Khvorostyanov, D. V., P. Ciais, G. Krinner, S. A. Zimov, C. Corradi, and G. Guggenberger (2008b), Vulnerability of permafrost carbon to global warming. Part II: Sensitivity of permafrost carbon stock to global warming, *Tellus B*, *60*, 265–275.
- Knoblauch, C., C. Beer, A. Sosnin, D. Wagner, and E. M. Pfeiffer (2013), Predicting long-term carbon mineralization and trace gas production from thawing permafrost of Northeast Siberia, *Glob. Chang. Biol.*, *19*, 1160–1172.
- Koven, C., P. Friedlingstein, P. Ciais, D. Khvorostyanov, G. Krinner, and C. Tarnocai (2009), On the formation of high-latitude soil carbon stocks: Effects of cryoturbation and insulation by organic matter in a land surface model, *Geophys. Res. Lett.*, *36*, L21501, doi:10.1029/2009GL040150.
- Koven, C. D., B. Ringeval, P. Friedlingstein, P. Ciais, P. Cadule, D. Khvorostyanov, G. Krinner, and C. Tarnocai (2011), Permafrost carbon-climate feedbacks accelerate global warming, *Proc. Natl. Acad. Sci. U. S. A.*, *108*, 14,769–14,774.
- Kowalczyk, E. A., Y. P. Wang, R. M. Law, H. L. Davies, J. L. McGregor, and G. Abramowitz (2006), The CSIRO Atmosphere Biosphere Land Exchange (CABLE) model for use in climate models and as an offline model, CSIRO Marine and Atmospheric Research Paper 013, CSIRO Marine and Atmospheric Research, 1615, 1616. [Available at http://www.cmar.csiro.au/e-print/open/kowalczyk_2006a.pdf]. [last access June 2011].
- Krinner, G., N. Viovy, N. de Noblet-Ducoudre, J. Ogee, J. Polcher, P. Friedlingstein, P. Ciais, S. Sitch, and I. C. Prentice (2005), A dynamic global vegetation model for studies of the coupled atmosphere-biosphere system, *Global Biogeochem. Cycles*, *19*, GB1015, doi:10.1029/2003GB002199.
- Langer, M., S. Westermann, S. Muster, K. Piel, and J. Boike (2011), The surface energy balance of a polygonal tundra site in northern Siberia—Part 1: Spring to fall, *Cryosphere*, *5*, 151–171.
- Leuning, R. (1990), Modelling stomatal behaviour and photosynthesis of *Eucalyptus grandis*, *Funct. Plant Biol.*, *17*, 159–175.
- Leuning, R. (1995), A critical-appraisal of a combined stomatal-photosynthesis model for C-3 Plants, *Plant Cell Environ.*, *18*, 339–355.
- Li, J., S. Ziegler, C. S. Lane, and S. A. Billings (2012), Warming-enhanced preferential microbial mineralization of humified boreal forest soil organic matter: Interpretation of soil profiles along a climate transect using laboratory incubations, *J. Geophys. Res.*, *117*, G02008, doi:10.1029/2011JG001769.
- Li, J., S. E. Ziegler, C. S. Lane, and S. A. Billings (2013), Legacies of native climate regime govern responses of boreal soil microbes to litter stoichiometry and temperature, *Soil Biol. Biochem.*, *66*, 204–213.
- Loth, B., H. F. Graf, and J. M. Oberhuber (1993), Snow cover model for global climate simulations, *J. Geophys. Res.*, *98*, 10,451–10,464.
- Lu, M., X. Zhou, Q. Yang, H. Li, Y. Luo, C. Fang, J. Chen, X. Yang, and B. Li (2012), Responses of ecosystem carbon cycle to experimental warming: A meta-analysis, *Ecology*, *94*, 726–738.
- Lu, X., Y.-P. Wang, T. Ziehn, and Y. Dai (2013), An efficient method for global parameter sensitivity analysis and its applications to the Australian community land surface model (CABLE), *Agr. Forest. Meteorol.*, *182–183*, 292–303.
- Luo, Y. Q. (2007), Terrestrial carbon-cycle feedback to climate warming, *Annu. Rev. Ecol. Evol. Syst.*, *38*, 683–712.
- MacDougall, A. H., C. A. Avis, and A. J. Weaver (2012), Significant contribution to climate warming from the permafrost carbon feedback, *Nat. Geosci.*, *5*, 719–721.
- McGuire, A. D., L. G. Anderson, T. R. Christensen, S. Dallimore, L. D. Guo, D. J. Hayes, M. Heimann, T. D. Lorenson, R. W. Macdonald, and N. Roulet (2009), Sensitivity of the carbon cycle in the Arctic to climate change, *Ecol. Monograph*, *79*, 523–555.
- McGuire, A. D., et al. (2012), An assessment of the carbon balance of Arctic tundra: Comparisons among observations, process models, and atmospheric inversions, *Biogeosciences*, *9*, 3185–3204.
- Merbold, L., W. L. Kutsch, C. Corradi, O. Kolle, C. Rebmann, P. C. Stoy, S. A. Zimov, and E. D. Schulze (2009), Artificial drainage and associated carbon fluxes (CO₂/CH₄) in a tundra ecosystem, *Glob. Chang. Biol.*, *15*, 2599–2614.
- Natali, S. M., E. A. G. Schuur, C. Trucco, C. E. H. Pries, K. G. Crummer, and A. F. B. Lopez (2011), Effects of experimental warming of air, soil and permafrost on carbon balance in Alaskan tundra, *Glob. Chang. Biol.*, *17*, 1394–1407.
- Natali, S. M., E. A. G. Schuur, and R. L. Rubin (2012), Increased plant productivity in Alaskan tundra as a result of experimental warming of soil and permafrost, *J. Ecol.*, *100*, 488–498.

- Natali, S. M., E. A. G. Schuur, E. E. Webb, C. E. Hicks Pries, and K. G. Crummer (2014), Permafrost degradation stimulates carbon loss from experimentally warmed tundra, *Ecology*, in press.
- Nelson, F. E. (2003), (Un)frozen in time, *Science*, *299*, 1673–1675.
- O'Donnell, J. A., J. W. Harden, A. D. McGuire, and V. E. Romanovsky (2011), Exploring the sensitivity of soil carbon dynamics to climate change, fire disturbance and permafrost thaw in a black spruce ecosystem, *Biogeosciences*, *8*, 1367–1382.
- Oleson, K. W., D. M. Lawrence, G. B. Bonan, M. G. Flanner, E. Kluzek, P. J. Lawrence, S. Levis, S. C. Swenson, and P. E. Thornton (2010), Technical description of version 4.0 of the Community Land Model, *Technical Note*, 258 pp., Natl. Cent. for Atmos. Res., Boulder, Colo.
- Osterkamp, T. E. (2007), Characteristics of the recent warming of permafrost in Alaska, *J. Geophys. Res.*, *112*, F02S02, doi:10.1029/2006JF000578.
- Osterkamp, T. E., and J. C. Jorgenson (2006), Warming of permafrost in the Arctic National Wildlife Refuge, Alaska, *Permafrost Periglacial Process.*, *17*, 65–69.
- Osterkamp, T. E., M. T. Jorgenson, E. A. G. Schuur, Y. L. Shur, M. Z. Kanevskiy, J. G. Vogel, and V. E. Tumskey (2009), Physical and ecological changes associated with warming permafrost and thermokarst in interior Alaska, *Permafrost Periglacial Process.*, *20*, 235–256.
- Parmentier, F. J. W., M. K. van der Molen, J. van Huissteden, S. A. Karsanaev, A. V. Kononov, D. A. Suzdalov, T. C. Maximov, and A. J. Dolman (2011), Longer growing seasons do not increase net carbon uptake in the northeastern Siberian tundra, *J. Geophys. Res.*, *116*, G04013, doi:10.1029/2011JG001653.
- Pries, C. E. H., E. A. G. Schuur, and K. G. Crummer (2013), Thawing permafrost increases old soil and autotrophic respiration in tundra: Partitioning ecosystem respiration using delta C-13 and Delta C-14, *Glob. Chang. Biol.*, *19*, 649–661.
- Reichstein, M., J. D. Tenhunen, O. Rouspard, J.-M. Ourcival, S. Rambal, F. Miglietta, A. Peressotti, M. Pecchiari, G. Tirone, and R. Valentini (2002), Severe drought effects on ecosystem CO₂ and H₂O fluxes at three Mediterranean evergreen sites: Revision of current hypotheses?, *Glob. Chang. Biol.*, *8*, 999–1017.
- Schaefer, K., T. Zhang, L. Bruhwiler, and A. P. Barrett (2011), Amount and timing of permafrost carbon release in response to climate warming, *Tellus B*, *63*, 165–180.
- Schneider von Deimling, T., M. Meinshausen, A. Levermann, V. Huber, K. Frieler, D. M. Lawrence, and V. Brovkin (2012), Estimating the near-surface permafrost-carbon feedback on global warming, *Biogeosciences*, *9*, 649–665.
- Schuur, E. A. G., et al. (2008), Vulnerability of permafrost carbon to climate change: Implications for the global carbon cycle, *BioScience*, *58*, 701–714.
- Schuur, E. A. G., J. G. Vogel, K. G. Crummer, H. Lee, J. O. Sickman, and T. E. Osterkamp (2009), The effect of permafrost thaw on old carbon release and net carbon exchange from tundra, *Nature*, *459*, 556–559.
- Schuur, E. A. G., et al. (2013), Expert assessment of vulnerability of permafrost carbon to climate change, *Clim. Change*, *119*, 359–374.
- Sellers, P. J., Y. Mintz, Y. C. Sud, and A. Dalcher (1986), A Simple Biosphere Model (Sib) for use within General-Circulation Models, *J. Atmos. Sci.*, *43*, 505–531.
- Shaver, G. R., et al. (2000), Global warming and terrestrial ecosystems: A conceptual framework for analysis, *BioScience*, *50*, 871–882.
- Smith, L. C., G. M. MacDonald, A. A. Velichko, D. W. Beilman, O. K. Borisova, K. E. Frey, K. V. Kremenetski, and Y. Sheng (2004), Siberian peatlands a net carbon sink and global methane source since the early Holocene, *Science*, *303*, 353–356.
- Smith, S. L., S. A. Wolfe, D. W. Riseborough, and F. M. Nixon (2009), Active-layer characteristics and summer climatic indices, Mackenzie Valley, Northwest Territories, Canada, *Permafrost Periglacial Process.*, *20*, 201–220.
- Stieglitz, M., S. J. Dery, V. E. Romanovsky, and T. E. Osterkamp (2003), The role of snow cover in the warming of arctic permafrost, *Geophys. Res. Lett.*, *30*(13), 1721, doi:10.1029/2003GL017337.
- Tang, J. Y., and Q. L. Zhuang (2011), Modeling soil thermal and hydrological dynamics and changes of growing season in Alaskan terrestrial ecosystems, *Clim. Change*, *107*, 481–510.
- Tarnocai, C., J. G. Canadell, E. A. G. Schuur, P. Kuhry, G. Mazhitova, and S. Zimov (2009), Soil organic carbon pools in the northern circumpolar permafrost region, *Global Biogeochem. Cycles*, *23*, GB2023, doi:10.1029/2008GB003327.
- Tjoelker, M. G., J. Oleksyn, and P. B. Reich (2001), Modelling respiration of vegetation: Evidence for a general temperature-dependent Q₁₀, *Glob. Chang. Biol.*, *7*, 223–230.
- Trucco, C., E. A. G. Schuur, S. M. Natali, E. F. Belshe, R. Bracho, and J. Vogel (2012), Seven-year trends of CO₂ exchange in a tundra ecosystem affected by long-term permafrost thaw, *J. Geophys. Res.*, *117*, G02031, doi:10.1029/2011JG001907.
- van Everdingen, R. (2005), *Multi-Language Glossary of Permafrost and Related Ground-Ice Terms*, National Snow and Ice Data Center/World Data Center for Glaciology, Boulder, Colo.
- van Huissteden, J., C. Berrittella, F. J. W. Parmentier, Y. Mi, T. C. Maximov, and A. J. Dolman (2011), Methane emissions from permafrost thaw lakes limited by lake drainage, *Nat. Clim. Change*, *1*, 119–123.
- von Deimling, T. S., M. Meinshausen, A. Levermann, V. Huber, K. Frieler, D. M. Lawrence, and V. Brovkin (2012), Estimating the near-surface permafrost-carbon feedback on global warming, *Biogeosciences*, *9*, 649–665.
- Waelbroeck, C., P. Monfray, W. C. Oechel, S. Hastings, and G. Vourlitis (1997), The impact of permafrost thawing on the carbon dynamics of tundra, *Geophys. Res. Lett.*, *24*, 229–232, doi:10.1029/97GL00071.
- Wang, Y. P., and R. Leuning (1998), A two-leaf model for canopy conductance, photosynthesis and partitioning of available energy. I: Model description and comparison with a multi-layered model, *Agr. Forest. Meteorol.*, *91*, 89–111.
- Wang, Y. P., D. Baldocchi, R. Leuning, E. Falge, and T. Vesala (2007), Estimating parameters in a land-surface model by applying nonlinear inversion to eddy covariance flux measurements from eight FLUXNET sites, *Glob. Chang. Biol.*, *13*, 652–670.
- Wang, Y. P., R. M. Law, and B. Pak (2010), A global model of carbon, nitrogen and phosphorus cycles for the terrestrial biosphere, *Biogeosciences*, *7*, 2261–2282.
- Wang, Y. P., E. Kowalczyk, R. Leuning, G. Abramowitz, M. R. Raupach, B. Pak, E. van Gorsel, and A. Luhr (2011), Diagnosing errors in a land surface model (CABLE) in the time and frequency domains, *J. Geophys. Res.*, *116*, G01034, doi:10.1029/2010JG001385.
- Weedon, J. T., G. A. Kowalchuk, R. Aerts, J. van Hal, R. van Logtestijn, N. Tas, W. F. M. Roling, and P. M. van Bodegom (2012), Summer warming accelerates sub-arctic peatland nitrogen cycling without changing enzyme pools or microbial community structure, *Glob. Chang. Biol.*, *18*, 138–150.
- Williams, P. J., and M. W. Smith (1989), *The Ground Thermal Regime. The Frozen Earth*, Cambridge Univ. Press, Cambridge.
- Wohlfahrt, G., M. Bahn, U. Tappeiner, and A. Cernusca (2001), A multi-component, multi-species model of vegetation-atmosphere CO₂ and energy exchange for mountain grasslands, *Agr. Forest. Meteorol.*, *106*, 261–287.
- Wu, Q., and T. Zhang (2010), Changes in active layer thickness over the Qinghai-Tibetan Plateau from 1995 to 2007, *J. Geophys. Res.*, *115*, D09107, doi:10.1029/2009JD012974.
- Xia, J. Y., Y. Q. Luo, Y. P. Wang, E. S. Weng, and O. Hararuk (2012), A semi-analytical solution to accelerate spin-up of a coupled carbon and nitrogen land model to steady state, *Geosci. Model Dev.*, *5*, 1259–1271.

- Xia, J., J. Chen, S. Piao, P. Ciais, Y. Luo, and S. Wan (2014), Terrestrial carbon cycle affected by non-uniform climate warming, *Nat. Geosci.*, *7*, 173–180.
- Yang, Z.-L., R. E. Dickinson, A. Robock, and K. Y. Vinnikov (1997), Validation of the snow submodel of the biosphere–atmosphere transfer scheme with Russian snow cover and meteorological observational data, *J. Climate*, *10*, 353–373.
- Zhang, T. J. (2005), Influence of the seasonal snow cover on the ground thermal regime: An overview, *Rev. Geophys.*, *43*, RG4002, doi:10.1029/2004RG000157.
- Zhang, Q., A. J. Pitman, Y. P. Wang, Y. Dai, and P. J. Lawrence (2013), The impact of nitrogen and phosphorous limitation on the estimated terrestrial carbon balance and warming of land use change over the last 156 yr, *Earth Syst. Dynam. Discuss.*, *4*, 507–539.
- Zhuang, Q., J. He, Y. Lu, L. Ji, J. Xiao, and T. Luo (2010), Carbon dynamics of terrestrial ecosystems on the Tibetan Plateau during the 20th century: An analysis with a process-based biogeochemical model, *Glob. Ecol. Biogeogr.*, *19*, 649–662.
- Zimov, S. A., S. P. Davidov, Y. V. Voropaev, S. F. Prosiannikov, I. P. Semiletov, M. C. Chapin, and F. S. Chapin (1996), Siberian CO₂ efflux in winter as a CO₂ source and cause of seasonality in atmospheric CO₂, *Clim. Change*, *33*, 111–120.
- Zimov, S. A., S. P. Davydov, G. M. Zimova, A. I. Davydova, E. A. G. Schuur, K. Dutta, and F. S. Chapin (2006a), Permafrost carbon: Stock and decomposability of a globally significant carbon pool, *Geophys. Res. Lett.*, *33*, L20502, doi:10.1029/2006GL027484.
- Zimov, S. A., E. A. G. Schuur, and F. S. Chapin (2006b), Permafrost and the global carbon budget, *Science*, *312*, 1612–1613.